AIChE

Measurement Based Modeling and Control of Bimodal Particle Size Distribution in Batch Emulsion Polymerization

Mazen Alamir
Gipsa-lab/CNRS, University of Grenoble. Rue de la Houille Blanche, 38400 Saint Martin d'Hères, France

Nida Sheibat-Othman and Sami Othman
Université de Lyon, Univ. Lyon 1, CPE Lyon, CNRS, UMR 5007, Laboratoire d'Automatique et de Génie des Procédés (LAGEP), 43 Bd du 11, F-69616 Villeurbanne, France

DOI 10.1002/aic.12148
Published online January 20, 2010 in Wiley InterScience (www.interscience.wiley.com).

In this article, a novel modeling approach is proposed for bimodal Particle Size Distribution (PSD) control in batch emulsion polymerization. The modeling approach is based on a behavioral model structure that captures the dynamics of PSD. The parameters of the resulting model can be easily identified using a limited number of experiments. The resulting model can then be incorporated in a simple learning scheme to produce a desired bimodal PSD while compensating for model mismatch and/or physical parameters variations using very simple updating rules. © 2010 American Institute of Chemical Engineers *AIChE J,* 56: 2122–2136, 2010
Keywords: polymerization in emulsion, reduced model, particle size distribution, nonlinear control, predictive control

Introduction

Emulsion polymerization processes are interesting for the production of adhesives and paints. The latex produced in these processes is the dispersion of polymer particles into water. The latex properties (optical properties, film formation) heavily depend on the particle size distribution (PSD) of the latex.[1] Particularly, the use of bimodal PSD was found interesting in increasing the solid content (which is of high interest in order to reduce the drying time and transport costs), while keeping a low latex viscosity (see for instance, Refs. 2 and 3).

In Refs. 4 and 5 the theoretical controllability of the population balance equations of this system has been analyzed. The authors concluded that the PSD is approximately controllable for unconstrained manipulation of feed surfactant concentration. Then, the authors used online measurements of the monomer conversion obtained by densimetry and delayed measurements of the particle size compensated by an observer to calculate the number of particles and predict the birth rate of particles in a continuous stirred tank reactor. These measurements were then used in a PID controller that manipulates the surfactant feed to control the PSD.

Despite the theoretically possible controllability of the system, and because of the lack of online measurements of the PSD, controlling the PSD remained a difficult task. Light scattering technologies mainly concern monodispersed lattices and operate off-line because of the necessity of dilution. However, the analysis time of such techniques can be reduced to about 5 minutes and might therefore be adapted for online use if a dilution system is incorporated in the process. Separative technologies, such as capillary hydrodynamic fractionation (CHDF) are more suitable for multidispersed lattices (see for instance[6] and[7]) but require a longer analysis time (about 15 minutes) and operate therefore off-line. An alternative measurement that can be useful for controlling the PSD is the concentration of the free surfactant in the aqueous phase (since it allows calculating the

Correspondence concerning this article should be addressed to M. Alamir at mazen.alamir@gipsa-lab.inpg.fr.

concentration of micelles) that can be obtained by conductimetry (see for instance[8]). However, for the moment, this technique is limited to diluted lattices and the maintenance of the probe is delicate. Besides, the correlations between the condcutimetry measurements and the concentration of surfactant in the aqueous phase have to be re-identified for every new system. This method was however considered (in a simulation study) in Ref. 9 to control the PSD by a PID controller.

In Ref. 10 a review of the different strategies used to obtain a bimodal PSD has been proposed. Nowadays, these strategies can be classified as follows (unless mentioned, all strategies are validated only by simulation). First of all, the effect of the operating policies on the PSD was studied in open-loop control strategies. For instance, in Ref. 11 the possibility of optimizing the surfactant flow rate to obtain a bimodal PSD has been investigated, whereas in Refs. 12 and 13 an open-loop genetic control algorithm to predict the control profiles to obtain the desired PSD of a copolymerization process has been proposed. The profiles so obtained were then applied to the process experimentally.

In parallel, direct control of the PSD was considered in some works assuming available online PSD measurement. An observer was usually incorporated to compensate the measurement delay. In Ref. 14 experimental investigation has been proposed for the simultaneous control of the PSD and molecular weight distribution by manipulating the flow rates of the monomers (styrene and methyl methacrylate), surfactant, initiator, and the temperature of the reactor. Off-line measurements of the monomer conversion by gravimetry, molecular weight distribution by gel permeation chromatography and PSD by Zetasizer and CHDF were used in a multivariable model predictive control algorithm to maximize the width of the PSD and the average number molecular weight. The lack and delay of measurements were overcome by using a soft-sensor.

Similarly, in Ref. 15 a mult-input multi-output predictive control strategy has been implemented experimentally to control the polydispersity of the PSD and the molecular weight distribution by manipulating the flow rate of monomer and the reactor temperature. The algorithm involved a linear model obtained off-line by linearization around an operating trajectory. The measurement of the PSD was obtained by off-line CHDF incorporated in a dynamic model that operated as a soft-sensor.

Different control laws to control the PSD in a semi-batch emulsion copolymerization reactor have been proposed in Ref. 16 using principal component analysis to obtain a reduced process model. They compared the PID and nonlinear predictive control using quadratic dynamic matrix controller (DMC). Two measurements have been used: the solid content (every minute) and the PSD measurement (available every 12 minutes). The delay of measurement was compensated by an extended Kalman filter.

In most of the above cited works related to PSD control, the control strategy is based on a physically meaningful mathematical model representing the nucleation, growth, and sometimes coagulation stages of the polymerization. It is well known however that this model is difficult to identify precisely because it includes a huge number of correlations and parameters, the fact that the phenomena of nucleation is significantly nonlinear and is sensitive to impurities. For instance, some parameters might have different values estimated in the literature (ex. the propagation rate of monomer). Moreover, there are quite often different correlations to represent the same phenomena available in the literature (ex. aggregation). In addition, changes in the properties of raw materials might considerably affect the reaction. For instance, any evolution in the surfactant nature (ex. aggregation), will lead to a change in the critical micelle concentration or the particle surface covered by a molecule of surfactant. However, these two parameters are crucial in the computation of the nucleation rate. For all these reasons, the control strategy has to be extremely robust to modeling errors.

In the case where the process model or parameters are not well known, batch-to-batch control allows taking into account model mismatches. The batch history permits the refinement of some process parameters or considering phenomena that are not present in the fundamental process model. Corrections can be incorporated directly in the fundamental process model or in a new simplified model. For instance, to take into account process variation, a midcourse correction of the surfactant concentration (by a shot) based on the predicted PSD by partial least square models that incorporate the available measurements has been proposed in Ref. 17 whereas in Ref. 18 a combination of the fundamental process model with a static partial least square model to account for modeling errors has been proposed. Assuming the measurement of the full PSD available on-line, the hybrid model-based approach was used for batch-to-batch control of the PSD. In this approach, the input trajectories were calculated by minimizing the error between the desired PSD and the one obtained from the hybrid model. This work was then investigated experimentally in Ref. 19). The batch-to-batch iterative feedback PSD control was also used in Ref. 20 although in this case corrections were incorporated directly in the fundamental process model. They considered as parameters to be updated: the critical micelle concentration, the propagation rate coefficient, the coagulation rate and the growth rate.

The Contribution of the Present Work: A Behavioral Model Approach

The contribution of this article is based on the conviction that modeling the different mechanisms that take place during emulsion polymerization is still an open issue. This task is made difficult by the complexity of these coupled and not yet completely understood mechanisms. Moreover, when using physical phenomenon to model the process, the resulting model generally depends on a high number of parameters and only a part of the phenomena being involved is taken into account. Therefore, there is no evidence that by updating the physical parameters of such a *partial* model, the effects of nonmodeled phenomena can be recovered.

Control scientists, dealing with modeling, identification and control of complex processes since already half a century, are now deeply convinced that from a control point of view:

A good model is a model that enables the task to be correctly achieved.

Following this simple statement, the quality of a given model is different when the task is to understand how nature does things? or when it is to answer the question what is to be done to enhance a desired result in a given process. In the first case, one needs generic, physically meaningful relationships while in the latter, experimentally identified behavioral models that capture the dynamics of the control-related features are sometimes more than sufficient.

Such behavioral models generally need a drastically less number of parameters that can reasonably be identified using available measurement. To cite an example, linear identified transfer functions that are based on least squares identification are completely decoupled from any physical understanding of the underlying real mechanism. However, nobody can deny all the history of successful applications of control achievement that are based on such models.

For more discussion on the behavioral approaches, interested readers may refer to.[21]

The contribution of this article falls in this last category. More precisely, we are interested in controlling the final particle size distribution in emulsion batch polymerization. The PSD is assumed to be measured during the batch operation with some sampling rate τ. More precisely, it is assumed that at each instant $t_k = k/\tau$, the following vector of measurement is available

$$F(t_k, r_i) \quad r_{\min} = r_1 < r_2 < \cdots < r_{n_r} = r_{\max} \tag{1}$$

where $F(t_k, r_i)$ is the number of particles of size r_i present in the reactor.

Using these measurements, a limited number of batch operations are performed and the related measurements are acquired. Each of these batch operations is defined by a precise controlled scenario (see the parameterized controlled batch operation section) with different set of parameters. The data obtained from these identification experiments are used to build up a simple behavioral model. The latter is incorporated in a rapidly convergent learning control scheme.

In all the results shown in the sequel, the mathematical model proposed in Ref. 22 plays the role of experimental facility to deliver the measurement data. For the sake of completeness, this model is described in the appendix. By doing so and provided that the following conditions are fulfilled:

- The algorithm uses no specific knowledge of the mathematical model that is used to produce the measurements;
- The validation scenarios use a detuned model that differs from the one used in the identification step, it can be legitimately inferred from the success of the proposed approach that is would rather be successful in pure experimental setting or at least that experimenting the solution using a real test bed facility is worthwhile.

The article is organized as follows: The definition of the basic parameterized Controlled Batch Operation (CBO) protocol is precisely defined in section the parameterized controlled batch operation. Section behavioral model of a CBO shows how a reduced behavioral model is built-up based on a few number of experimental CBO's with different set of parameters. The use of the behavioral model so obtained in a learning control scheme to compensate for model mismatches and/or process variability is shown in incorporating the behavioral model in a simple learning control scheme section. Finally, some validating scenarios are proposed in numerical simulations section to show the efficiency of the whole proposed scheme.

The Parameterized Controlled Batch Operation

The parameterized Controlled Batch Operation (CBO) is a batch session in which the temporal structure of decisions is already defined up to a reduced set of paramaters. Note that by Controlled Batch Operation, it is referred to the fact that in the very definition of the scheduled sequence of actions, feedback is already present. More precisely, this means that the time structure of the decision depends on on-line measurements and is not a simple sequence of actions that are labeled in time.

More precisely, the CBO is composed of three phases that are described below (see Figure 1):

- PHASE 1 starts with a predefined initial state with no surfactant injection ($Q_s = 0$) until the minimum radius measurement $F(t_1, r_1)$ vanishes at some instant t_1. During PHASE 1, a first population is created that moves to the right in the axis of radius. Note that the instant t_1 (see Figure 1) is not known in advance but is defined by the measurement related inequality

$$F(t_1, r_1) \leq \varepsilon_1 \tag{2}$$

- PHASE 2 starts δ time units after condition (2) is satisfied, namely at instant $t_1 + \delta$ (see Figure 1). From this instant and until the end of PHASE 2, a surfactant flow rate $Q_s = Q_s^0$ is injected. The delay δ and the value of the flow rate Q_s^0 are the two parameters that define the CBO, namely:

$$p := \begin{pmatrix} \delta \\ Q_s^0 \end{pmatrix} \in \mathbb{R}_+^2$$

where $\mathbb{R}_+ = [0, \infty]$.

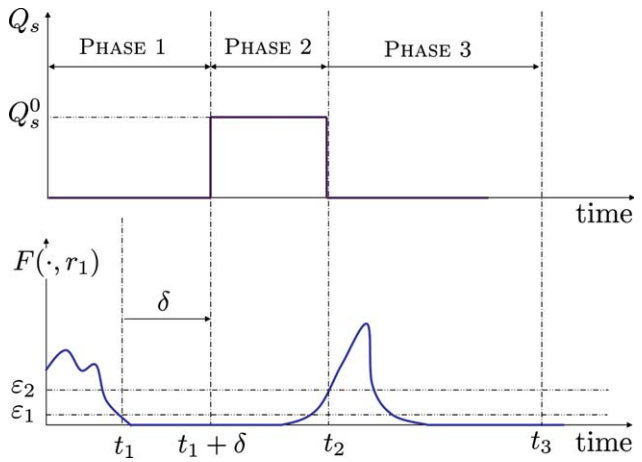

Figure 1. Schematic view of the Controlled Batch Operation.

Note that the different phases are defined by measurement driven firing instants. In what follows, the thresholds ε_1 and ε_2 are defined once for all while the delay δ and the flow rate value Q_s^0 are decision variables that are decided on line based on both measurements and desired PSD. [Color figure can be viewed in the online issue, which is available at www.interscience.wiley.com.]

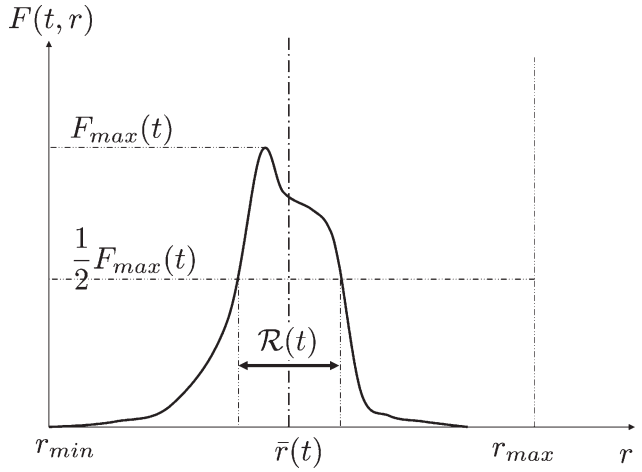

Figure 2. Definition of the position $\bar{r}(t)$ of a single mode.

• It is readily understandable that the amount of delay $\boldsymbol{\delta}$ is a key parameter in controlling the distance between the two populations of the bimodal distribution on the axis of radius. Mastering the value of $\boldsymbol{\delta}$ is a key issue in the success of the whole operation.

• The value of the surfactant flow-rate Q_s^0 during PHASE 2 is the second parameter that defines the CBO protocol since it has effects on both the amplitude of the latest population as well as the *growing rates* of both populations.

Although PHASE 2 is fired (at instant $t_1 + \delta$), the nucleation rate R_{nuc} remains at 0 during an amount of time that depends on rather complicated processes (PSD of the first mode, critical micelle concentration, presence of droplets, impurities, surfactant nature, etc.) until the nucleation rate wakes up and takes strictly non vanishing values. PHASE 2 ends at instant t_2 that corresponds to the measurement $F(t_2, r_1)$ going beyond some threshold ε_2 (see Figure 1):

$$F(t_2, r_1) \geq \varepsilon_2 \tag{3}$$

• Phase 3 starts then at instant t_2 from which the flow rate Q_s is reset to 0 until the end of the batch operation. This phase corresponds to measurability of the latest population that moves to the right on the axis of radius. This last phase of the CBO protocol is stopped when appropriate, say at some instant t_3 according to the desired bimodal PSD (see later).

Behavioral Model of a CBO

A behavioral model is a model that describes the evolution of the key quantities that are related to the underlying problem. When controlling a bimodal PSD, it is clear that the key quantities are the positions of the two modes on the axis of radius as well as the amplitude of the latest mode. However, this definition is rather vague and building a behavioral model needs this notion to be more precisely defined. This is the aim of the following section.

The positions of modes

For clarity, let us first consider the case where a single mode is present in the reactor (see Figure 2). In this case, the position $\bar{r}(t)$ at instant t is defined rigorously as follows:

$$\bar{r}(t) \ := \text{median}\, \mathcal{R}(t) \tag{4}$$

where $\mathcal{R}(t) \subset [r_{\min}, r_{\max}]$ is the subset defined by:

$$\mathcal{R}(t) = \left\{ r \in [r_{\min}, r_{\max}] \quad | \quad F(t,r) \geq \frac{1}{2} F_{\max}(t) \right\} \tag{5}$$

in which

$$F_{\max}(t) = \max_{r \in [r_{\min}, r_{\max}]} [F(t,r)] \tag{6}$$

In the case where two modes are present in the reactor, the definition may be easily extended by defining $r_{\min}^{(i)}$ and $r_{\max}^{(i)}$ for each mode $i \in \{1, 2\}$ (Figure 3), namely:

$$\bar{r}_i(t) = \text{median}\, \mathcal{R}_i(t) \tag{7}$$

$$\mathcal{R}_i(t) := \left\{ r \in [r_{\min}^{(i)}, r_{\max}^{(i)}] \quad | F(t,r) \geq \frac{1}{2} F_{\max}^{(i)}(t) \right\} \tag{8}$$

where:

$$r_{\min}^{(2)}(t) = r_{\min}$$
$$r_{\max}^{(1)}(t) = r_{\max}$$
$$r_{\max}^{(2)}(t) = r_{\min}^{(1)}(t) = \frac{1}{2}(\tilde{r}_1(t) + \tilde{r}_2(t))$$
$$\tilde{r}_i(t) = \text{Maximum population radius for mode } i$$
$$F_{\max}^{(i)}(t) = \text{maximum of the population } i$$

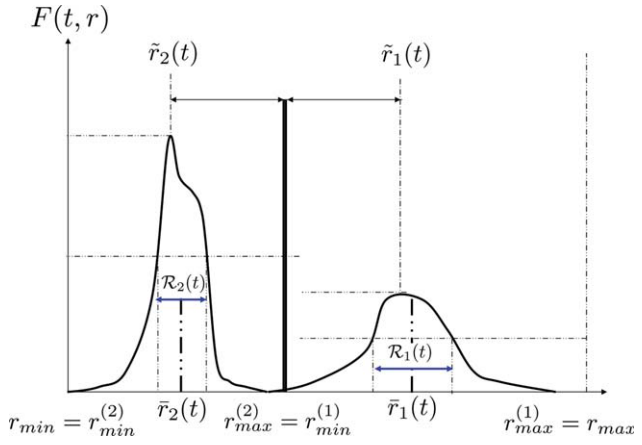

Figure 3. Definition of the position $\bar{r}(t)$ of a bimodal PSD.

[Color figure can be viewed in the online issue, which is available at www.interscience.wiley.com.]

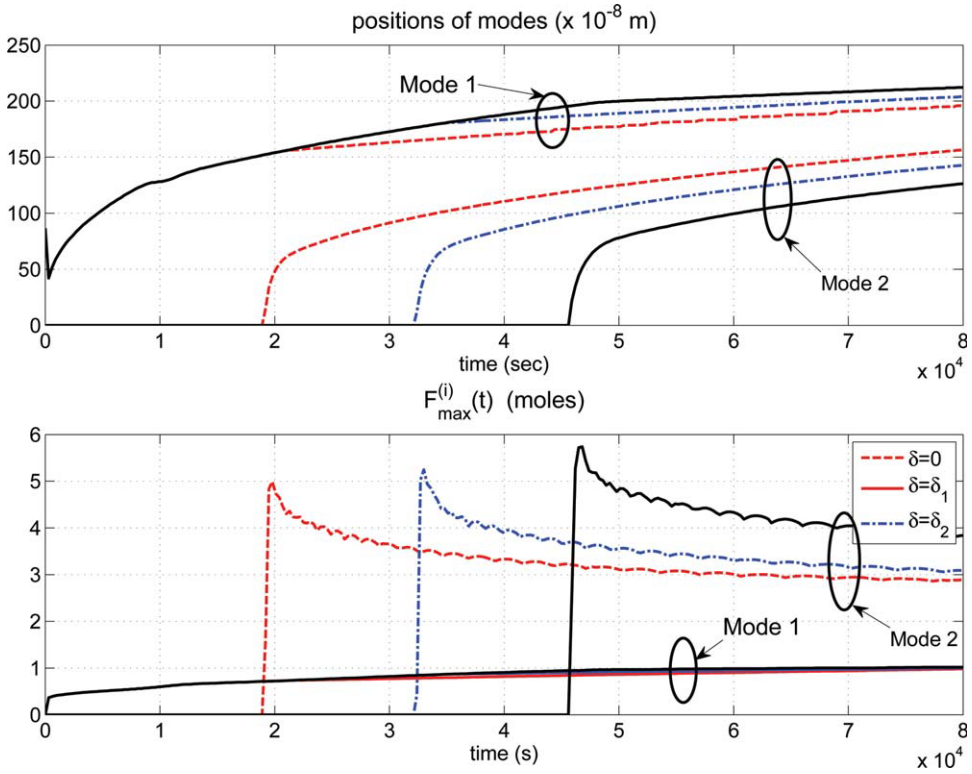

Figure 4. Evolution of the mode positions $\bar{r}_i(t)$ and the maximum population per mode under a fixed surfactant flow rate value $Q_s^0 = 5 \times 10^{-5}$ mol/s and different values of the delay $\delta \in \{0, 40{\cdot}\tau, 80{\cdot}\tau\}$ respectively represented using (red-dashed), (blue dash-dotted) and (black-solid) lines; τ = 300 s.

[Color figure can be viewed in the online issue, which is available at www.interscience.wiley.com.]

Parametrization of the temporal profiles

The behavioral model we are looking to identify from the measurements is the one that gives for a given choice of (δ, Q_s^0), the evolution of the variables

$$\bar{r}_1(\cdot) \quad ; \quad \bar{r}_2(\cdot) \quad ; \quad F_2(\cdot)$$

during the CBO. Let us first run few CBO's with different values of (δ, Q_s^0) that belong to the discrete set:

$$\mathcal{I} := \{(\delta, Q_s^0) \in \Delta \times \mathcal{Q}\} \tag{9}$$

where $\Delta = \{0, \delta_1, \delta_2\}$ and $\mathcal{Q} = \{Q_1, Q_2, Q_3\}$. Namely, the identification set contains for each of the two variables one low value, one medium value and one high value.

Figures 4 and 5 show the evolution of key variables $\bar{r}_i$ and $F_{\max}^{(i)}$ during the CBO's for different values of the pair (δ, Q_s^0). More precisely:

- Figure 4 shows the result for a given value of the surfactant flow rate Q_s^0 and different values of the delay δ. For a higher delay, the latest mode is created later and the first mode goes faster during the delay period. Note also how later modes are slightly higher than earlier ones.
- Figure 5 shows the result for a given delay δ and different values of the surfactant flow rate Q_s^0. Note that when the flow rate increases, the latest mode is created earlier, $F_{\max}$ increases but the two modes slow down.

Having this analysis in mind, one can go further in building the behavioral model. To do so, one needs to write the time-profiles $\bar{r}_1(\cdot)$, $\bar{r}_2(\cdot)$ and $F_{\max}^{(2)}(\cdot)$ using a low dimensional vector of parameters, say $\alpha \in \mathbb{R}^{n\alpha}$, namely:

$$\bar{r}_i(t) = \phi_i^r(t, \alpha) \quad ; \quad F_{\max}^{(i)}(t) = \phi_i^F(t, \alpha) \tag{10}$$

in such a way that the parameter vector α depends on the CBO's parameter $p = (\delta, Q_s^0)$. The behavioral model is then obtained by using the values of α for all the pairs $p = (\delta, Q_s^0)$ belonging to the identification set $\mathcal{I}$ defined by (9) to obtain a 2D Spline-based approximation of α for any different pairs of CBO's parameters p, namely:

$$\alpha(p) := \mathcal{S}\left(p, \{p^{(i)}\}_{i=1}^{\mathrm{card}(\mathcal{I})}\right); \quad p = (\delta, Q_s^0) \tag{11}$$

where $\mathrm{card}(\mathcal{I})$ is the number of elements of the discrete set $\mathcal{I}$. Having this Spline approximation, it is possible to predict the time evolution of the key quantities for any pair $p = (\delta, Q_s^0)$ that are no more necessarily in the identification set $\mathcal{I}$ according to:

$$\bar{r}_i(t) = \phi_i^r(t, \alpha(p)) \quad ; \quad F_{\max}^{(i)}(t) = \phi_i^F(t, \alpha(p)) \tag{12}$$

At this stage, it is crucial to make it clear that the model given by (12) holds only when using the CBO described

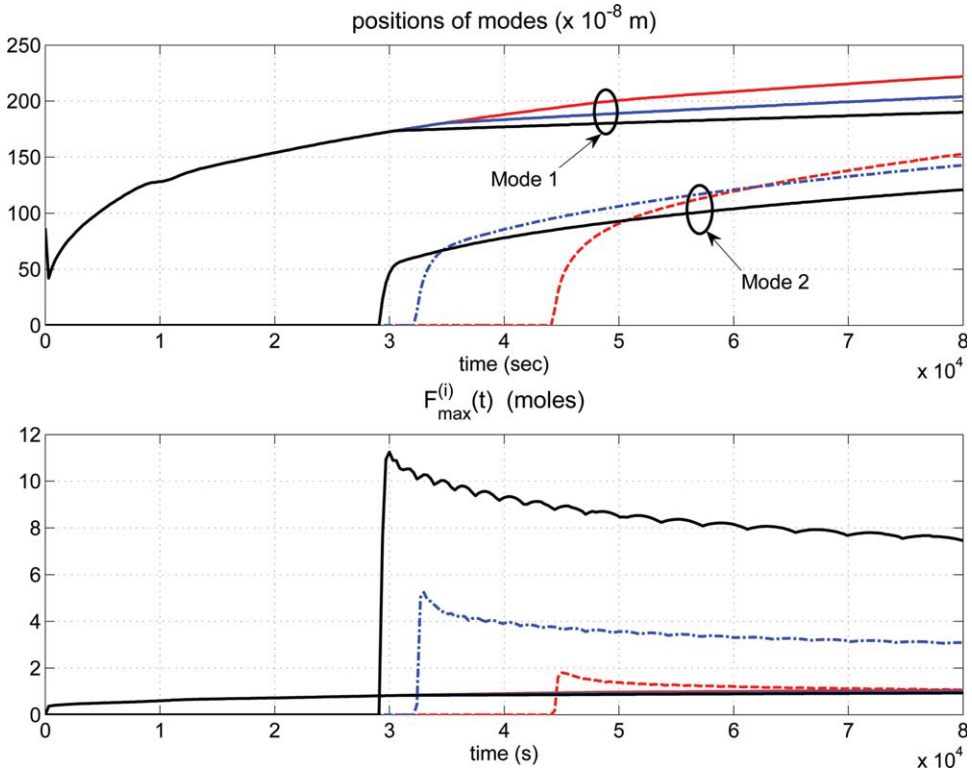

Figure 5. Evolution of the mode positions $\bar{r}_i(t)$ and the maximum population per mode under a fixed delay $\delta = 40\ \tau$ and different values of the surfactant flow rate $Q_s^0 \in \{2 \times 10^{-5}$ mol/sec, 5×10^{-5} mol/sec, 10×10^{-5} mol/sec$\}$ respectively represented using (red-dashed), (blue dash-dotted) and (black-solid) lines.

[Color figure can be viewed in the online issue, which is available at www.interscience.wiley.com.]

above. It is by no mean an open-loop model that may describe the behavior of the process for any control profile. This precisely implements the idea of the introduction according to which, the model has to be adapted to the task one is achieving.

Now, it remains to give a precise parametrization of the form (10) based on the experimental curves depicted in Figures 4 and 5.

Remark 1. *Note that only $\bar{r}_1(\cdot)$, $\bar{r}_2(\cdot)$ and $F^{(2)}_{max}(\cdot)$ need to be identified since the amplitude of the first mode seems to be quite insensitive to $p = (\delta, Q_s^0)$ as can be easily seen on Figures 4 and 5. This is quite expectable since we assumed that the initial conditions are fixed once for all and that during the first phase of the CBO, no surfactant injection is applied. This roughly determines the amplitude of the first mode although one can still act on its apparent velocity across the axis of radius.*

Remark 2. *It is worth underlying that the values of δ and Q_s^0 used to define $\mathcal{I}$ must be chosen such that for any possible set-point of interest, the corresponding pair (δ, Q_s^0) lies within the interpolation set $\mathcal{I}$. Moreover, for the interpolation to correctly represent the system behavior, it is implicitly assumed that no discontinuous bifurcation on the behavior of the system when (δ, Q_s^0) varies.*

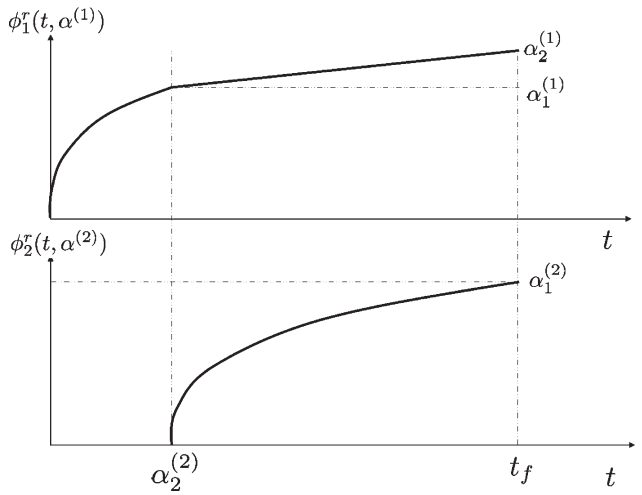

Figure 6. Schematic view of the parametrization function $\phi_i^r(t, \alpha)$ used to obtain a reduced dimensional parametrization of the time profiles $\bar{r}_1(t)$ and $\bar{r}_2(t)$.

Consequently only the four parameters $\alpha_1^{(1)}$, $\alpha_2^{(1)}$, $\alpha_1^{(2)}$ and $\alpha_2^{(2)}$ have to be calculated as a function of the CBO's parameter vector $p = (\delta, Q_s^0)$.

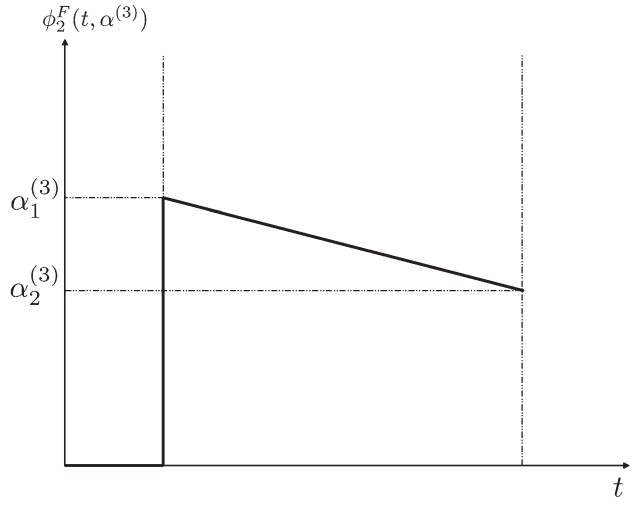

Figure 7. Schematic view of the parametrization function $\phi_i^F(t, \alpha)$ used to obtain a reduced dimensional parametrization of the evolution of the amplitude of the latest mode during the CBO's.

Consequently, only the two parameters $\alpha_1^{(3)}$ and $\alpha_2^{(3)}$ have to be computed in terms of the CBO's parameter vector $p = (\delta, Q_s^0)$.

Based on the time profiles of $\bar{r}_2$, the following parametrization can be used to approximate the evolution of this variable during the batch operation $[0, t_f]$ (see Figure 6):

$$\phi_2(t,\alpha) := \begin{cases} 0 & \text{if } t \le \alpha_2^{(2)} \\ \alpha_1^{(2)} \cdot \left[\frac{t-\alpha_2^{(2)}}{t_f-\alpha_2^{(2)}}\right]^{\frac{1}{3}} & \text{otherwise} \end{cases} \tag{13}$$

As for $\bar{r}_1$, note that it takes the same form as $\bar{r}_2$ except from the fact that just after the creation of the latest mode, the curve is interrupted and a straight line is to be used until the end of the batch operation. This comes from the change in the dynamics of mode 1 affected by the creation of the second mode. This leads to the following parametrization (see Figure 6):

$$\phi_1(t,\alpha) = \begin{cases} \alpha_1^{(1)} \cdot \left[\frac{t}{\alpha_2^{(2)}}\right]^{\frac{1}{3}} & \text{if } t \le \alpha_2^{(2)} \\ \alpha_1^{(1)} + \frac{t-\alpha_2^{(2)}}{t_f-\alpha_2^{(2)}} \cdot \left[\alpha_2^{(1)} - \alpha_1^{(1)}\right] & \text{otherwise} \end{cases} \tag{14}$$

Finally, the evolution of the amplitude of the latest mode, namely $F_{\max}^{(2)}$ can be roughly approximated according to the schematic view depicted on Figure 7 that leads to the following formulation:

$$\phi_2^F(t,\alpha) = \begin{cases} 0 & \text{if } t \le \alpha_2^{(2)} \\ \alpha_1^{(3)} + \frac{t-\alpha_2^{(2)}}{t_f-\alpha_2^{(2)}} \cdot \left[\alpha_2^{(3)} - \alpha_1^{(3)}\right] & \end{cases} \tag{15}$$

To summarize, the vector of parameters α invoked in (10), (11) and (12) is composed of six components and is given by:

$$\alpha = \left(\alpha_1^{(1)}, \alpha_2^{(1)}, \alpha_1^{(2)}, \alpha_2^{(2)}, \alpha_1^{(3)}, \alpha_2^{(3)}\right) \in \mathbb{R}^6 \tag{16}$$

Figures 8 and 9 show the comparison between the time profiles issued from the simulation of the model proposed in Ref. 22 (serving here as the experimental data generator) and the profiles issued from the mathematical behavioral model's expressions (13)-(15). Note that the precision of the approximation of $F_{\max}^{(2)}(\cdot)$ can be improved by introducing higher order polynomial rather than using a straight line as in (15). This can be easily done if appropriate.

This completes the definition of the behavioral model during a CBO. In the following section, the way this behavioral model can be incorporated in a simple learning control scheme is explained.

Incorporating the Behavioral Model in a Simple Learning Control Scheme

Although the behavioral model presented above is based on experimental identification, some model mismatches and uncertainties are to be expected. Moreover, the same system may show different behaviors when the environmental conditions evolve and/or when the hardware gets older. Note finally, that the behavioral model is still a rough approximation of the reality since it is based on spline like interpolation using only nine isolated experiments. This section proposes a self-contained learning and adaptation scheme that enables to recover these imperfections when dealing with a new PSD set-point to be produced.

The learning scheme takes the form of successive CBO's that iteratively improve the produced PSD using an extremely simple updating rule. This scheme is explained step-by-step in the following items:

(i) Assume that a new PSD set-point $(\bar{r}_1^d, \bar{r}_2^d, F_2^d)$ is given. The first CBO is executed using the parameters $p^{(1)}$ computed according to:

$$p^{(1)} := \arg\min_p J(p) := \min_t \left\| \begin{pmatrix} \phi_1^{\mathrm{r}}(t,\alpha(p)) - \bar{r}_1^{\mathrm{d}} \\ \phi_2^{\mathrm{r}}(t,\alpha(p)) - \bar{r}_2^{\mathrm{d}} \\ \phi_1^{\mathrm{F}}(t,\alpha(p)) - F_2^{\mathrm{d}} \end{pmatrix} \right\|_Q \tag{17}$$

namely, $p^{(1)}$ is chosen to minimize the difference between the characteristics of the desired PSD and the closest predicted PSD that will be obtained at some future time instant. The norm $\|\cdot\|_Q$ is the classical L_2 norm while Q is a diagonal matrix defined in such a way that the weighted components of the vector represent the relative error on desired values, namely:

$$Q = \mathrm{diag}\left(\frac{1}{\bar{r}_1^{\mathrm{d}}}, \frac{1}{\bar{r}_2^{\mathrm{d}}}, \frac{1}{F_2^{\mathrm{d}}}\right)$$

(ii) The corresponding CBO is executed using the parameter vector $p^{(1)}$, the third phase is stopped at instant $t_3^{(1)}$ which is defined as the first sampling instant for which the following condition is satisfied:

$$\bar{r}_2^{\mathrm{m}}(t_3^{(1)}) \ge \bar{r}_2^{\mathrm{d}} \tag{18}$$

where $\bar{r}_2^m$ denotes the measured position of the earliest mode.

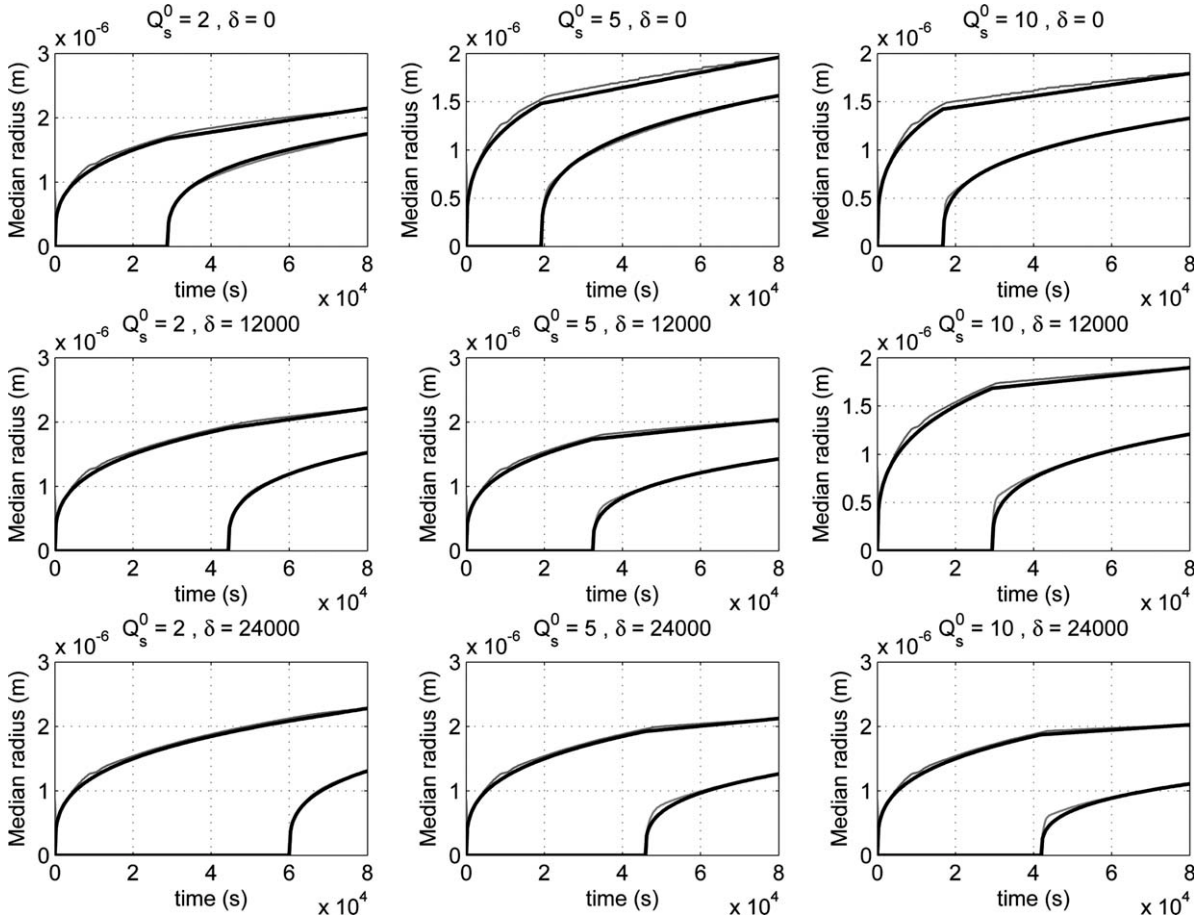

Figure 8. Positions of the modes on the radius axis during the CBO's for different pairs of values (δ, Q_s^0): Comparison between the simulation profiles (thin lines) and the profiles issued from the mathematical expressions (13)–(14) of the behavioral model (thick lines) for each mode.

(iii) At this instant, the following errors are measured:

$$\varepsilon_i^{(1)} = \bar{r}_i^{\mathrm{m}}(t_3^{(1)}) - \bar{r}_i^{\mathrm{d}} \tag{19}$$

$$\varepsilon_F^{(1)} = F_{\max}^{2,m}(t_3^{(1)}) - F_2^{\mathrm{d}} \tag{20}$$

(iv) These errors are interpreted as prediction errors of the behavioral model. The latter is therefore corrected according to:

$$\tilde{\phi}_i^r(t,\alpha(p)) = \phi_i^r(t,\alpha(p)) + \eta_i^{(2)} \tag{21}$$

$$\tilde{\phi}_2^F(t,\alpha(p)) = \phi_2^F(t,\alpha(p)) + \xi^{(2)} \tag{22}$$

where

$$\eta_i^{(2)} = \eta_i^{(1)} + \varepsilon_i^{(1)} \tag{23}$$

$$\xi^{(2)} = \xi^{(1)} + \varepsilon_F^{(1)} \tag{24}$$

where $\eta_i^{(1)}$ and $\xi^{(1)}$ are initially fixed to 0 but kept in the above formulae for clarity.

(v) The second CBO is now executed with the corrected model (21)–(22). Namely, the CBO parameter vector $p^{(2)}$ is computed according to:

$$p^{(2)} := \arg\min_p J(p) := \min_t \left\| \begin{pmatrix} \phi_1^r(t,\alpha(p)) + \eta_1^{(2)} - \bar{r}_1^d \\ \phi_2^r(t,\alpha(p)) + \eta_2^{(2)} - \bar{r}_2^d \\ \phi_1^F(t,\alpha(p)) + \xi^{(2)} - F_2^d \end{pmatrix} \right\|_Q \tag{25}$$

(vi) The procedure explained above is now repeated from step (2) on. The model is corrected accordingly and the next CBO is executed with the updated model.

The above discussion can be summarized as follows:

- The correction terms $\eta^{(1)}$ and $\xi^{(1)}$ are initialized to 0.
- The k-th CBO uses the following optimization problem to compute its parameter vector $p^{(k)}$:

$$p^{(k)} := \arg\min_p J(p) := \min_t \left\| \begin{pmatrix} \phi_1^r(t,\alpha(p)) + \eta_1^{(k)} - \bar{r}_1^d \\ \phi_2^r(t,\alpha(p)) + \eta_2^{(k)} - \bar{r}_2^d \\ \phi_1^F(t,\alpha(p)) + \xi^{(k)} - F_2^d \end{pmatrix} \right\|_Q \tag{26}$$

and it is stopped at the first instant $t_3^{(k)}$ satisfying

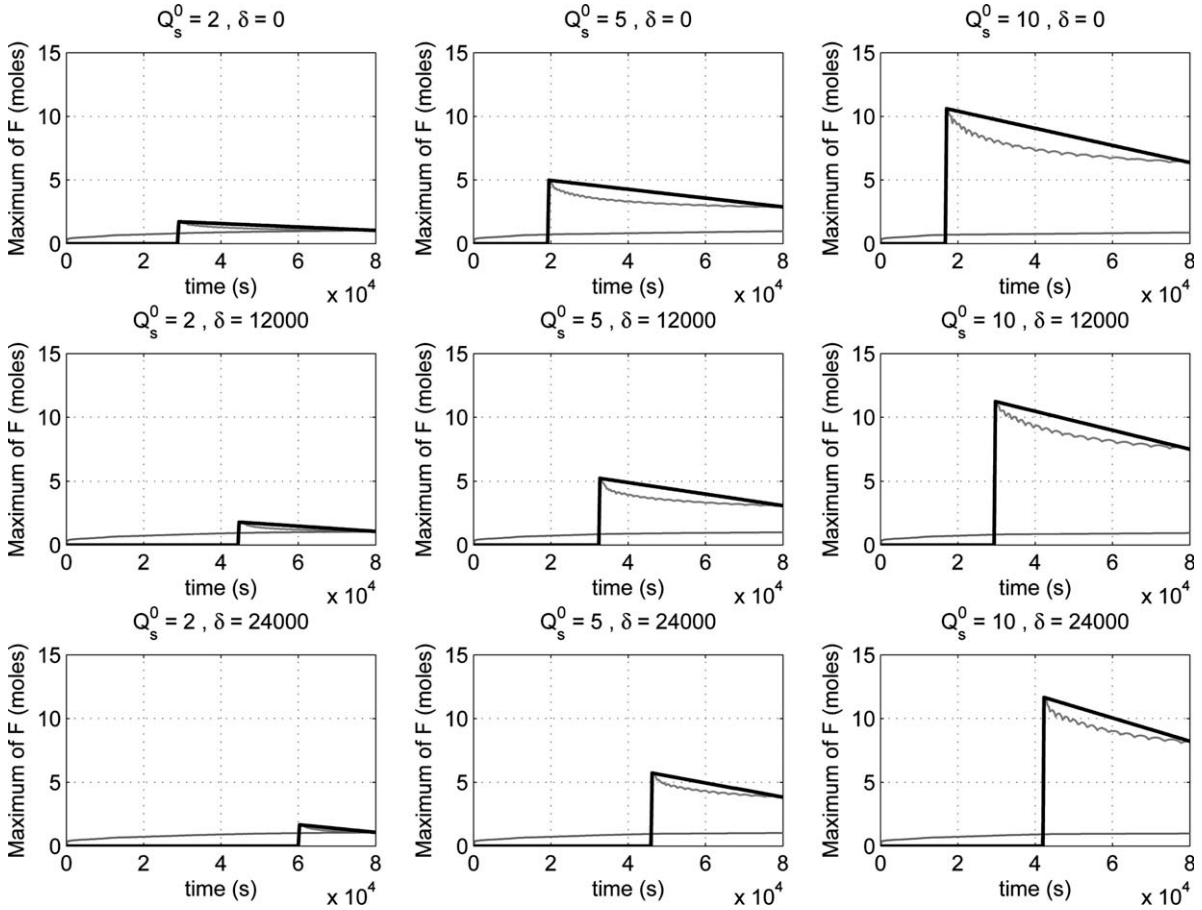

Figure 9. Maximum amplitude of the latest mode during the CBO's for different pairs of values (δ, Q_s^0): Comparison between the simulation profiles (thin lines) and the profiles issued from the mathematical expressions (15) of the behavioral model (thick lines).

The approximation can be easily improved by using second order polynomial in (15).

$$\bar{r}_2^{\mathrm{m}}(t_3^{(k)}) \geq \bar{r}_2^d \tag{27}$$

• At the end of the k-th CBO, the correction terms are updated according to:

$$\eta_i^{(k+1)} = \eta_i^{(k)} + \left[\bar{r}_1^m(t_3^{(k)}) - \bar{r}_1^d\right] \tag{28}$$

$$\xi^{(k+1)} = \xi^{(k)} + \left[F_{\max}^{2,m}(t_3^{(k)}) - F_2^d\right] \tag{29}$$

Effect of Measurement Noise

The noise affects the proposed scheme in two ways and at different stages of the process

• First, at the stage when the spline approximation is computed since this computation is based on the measurement based curves that have to be fitted. The effect of measurement noise at this stage is not critical since this computations are performed off line and appropriate filtering and pre-shaping of the measured curves can be carefully realized.

• During the Controlled Batch Operation, the measurement noise may affect the precision of the events detections that are used to start the delay temporization before the Phase 2 is fired at one hand and the firing of Phase 3. Taking not too small values of ε_1 and ε_2 renders the solution less sensitive to measurement noise. On the other hand, taking too high values of these thresholds may reduce the set of achievable PSD. The optimal choice is clearly noise dependent and more quantitative discussion needs concrete measurement of the noise.

Numerical Simulations

Light-scattering technique needs a sampling period of few minutes. In our case, we consider a sampling period of 300 seconds. This rather high value of the sampling periods leads to relatively high detection errors of the zero-crossing instants needed to fire the surfactant injection flow rate as well as to stop this injection. This feature has to be kept in mind when appreciating the results shown in this section. The optimization task has been performed using a uniform grid to discretize the convex hull conv($\mathcal{I}$) of the set $\mathcal{I}$.

Let us consider an experiment in which the desired values defining the PSD are given by:

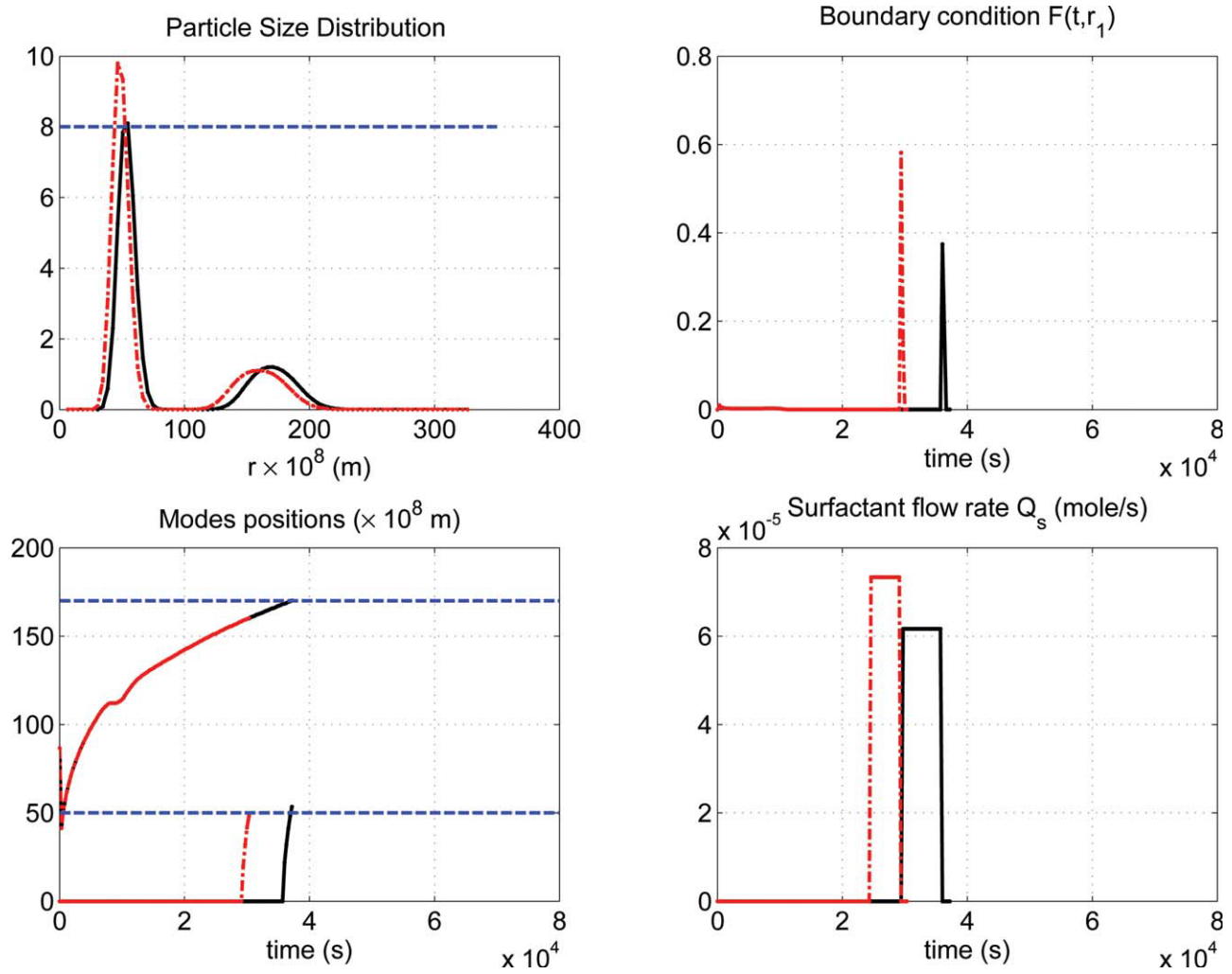

Figure 10. Evaluation of the learning control scheme proposed in section 5 using an erroneous model. This is obtained by changing the coefficients Kp_{11} and Kp_{12} of the model proposed by[22] used here to produce the measurement data.

Two batch operations (first in red-dotted and the second in black solid lines) were needed to recover the quality of the desired PSD that corresponds to CBO's parameter values that are not in the data used to identify the behavioral model. [Color figure can be viewed in the online issue, which is available at www.interscience.wiley.com.]

$$\bar{r}_1^d = 170 \times 10^{-8} m;\ \bar{r}_2^d = 50 \times 10^{-8} m;\ F_{\max}^d = 8\,\text{mol}$$

To make the simulated model different from the one that has been used to generate the measurement used in the identification process of the behavioral model, we changed two of the propagation rate coefficients of the model (namely K_{p11} and K_{p12}) by 30% and 20% respectively.

Figure 10 shows the results of the two first successive batch operations as introduced in section 5. Notice how the first batch operation while quite good as a first trial shows noticeable errors on all the requirements (positions of the mode as well as the amplitude of the latest mode). Note however how the next iteration recover the error thanks to the very simple updating rules (28), (29).

The CBO's parameter vector used in the second batch operation are given by:

$$p^{(2)} = (Q_s^0, \delta) = (6.17 \times 10^{-5}, 53.34 \times \tau) \qquad (30)$$

which corresponds to an interpolation inside the discrete set used in the identification step.

Figure 11 shows the same kind of results with the desired PSD given by:

$$\bar{r}_1^d = 180 \times 10^{-8} \quad ; \quad \bar{r}_2^d = 70 \times 10^{-8} \quad ; \quad F_{\max}^d = 2$$

Finally, Figure 12 shows a scenario where 3 batch operations were necessary because of a stronger modification of the model (50% decrease in the propagation rate parameters). The desired PSD is defined by:

$$\bar{r}_1^d = 190 \times 10^{-8} \quad ; \quad \bar{r}_2^d = 80 \times 10^{-8} \quad ; \quad F_{\max}^d = 3$$

Note how the initial PSD showed a first mode around 200×10^{-8} and quite small amplitude for the latest mode. The second batch corrects the positions of the mode but introduces too high amplitude for the latest mode. The third batch

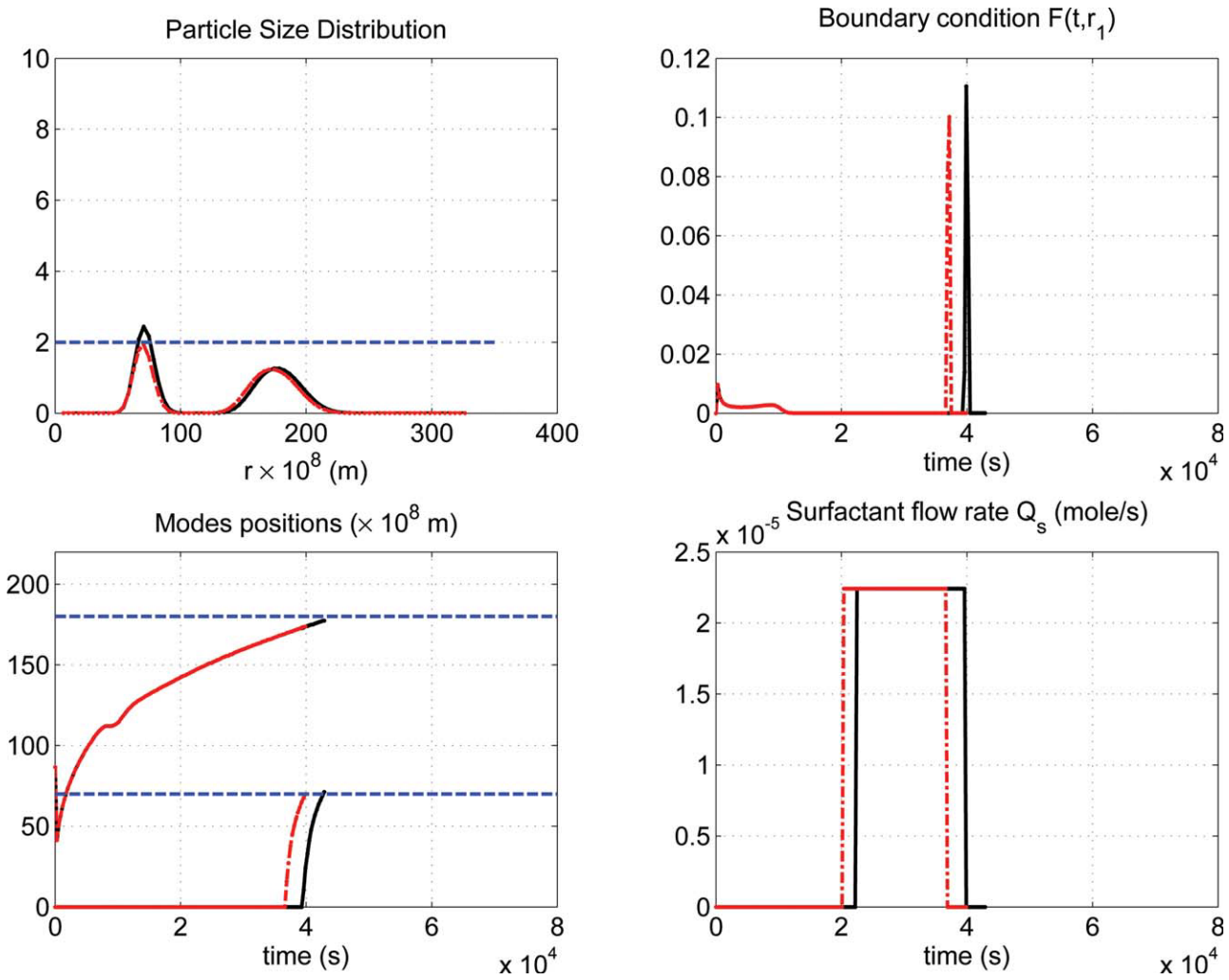

Figure 11. Same illustration as Figure 10 using different desired PSD (first batch in red-dotted, second batch in black-solid line).

Note how the behavioral model enables to capture both the modes positions as well as the amplitude of the latest mode. More precise model of the amplitude may increase the precision of the goal achievement. [Color figure can be viewed in the online issue, which is available at www.interscience.wiley.com.]

maintained the good positions of the modes and produced a much closer amplitude to the desired value.

Conclusions and Future Work

In this paper, a practical scheme is proposed for modeling and control of bimodal PSD in emulsion polymerization. The scheme is based on a simple behavioral model that can be easily identified from PSD discrete measurements using a few number of preliminary Controlled Batch Operations CBO. The behavioral model is then used in a repetitive learning control scheme to compensate for model mismatches and/or parameter change with time. The whole scheme is tested using the rather involved model proposed in Ref. 22 as a measurement generator. One way to enforce the performance of the proposed scheme is to iteratively enrich the database used to compute the spline by the new data issued from each batch operation. A forgetting factor can also be added to take into account the effects because of the process being getting older

It is needless to say that the only satisfactory validation is experimental since unlike simulation, two successive CBO's using the same parameters would never give the same results. Nevertheless, the result of the present paper suggests that simple behavioral model may faithfully capture the basic features that condition the success of the bimodal PSD control. Moreover, the proposed formulation set a simple formalism for batch-to-batch learning that involves few parameters and extremely simple updating rules.

It remains however true that the suggested scheme is one option among many others. The definition of a CBO may be done in too many ways. In that sense, the paper can be viewed as a starting point to explore different kind of parametrization of CBO. in particular, CBO's may involve more

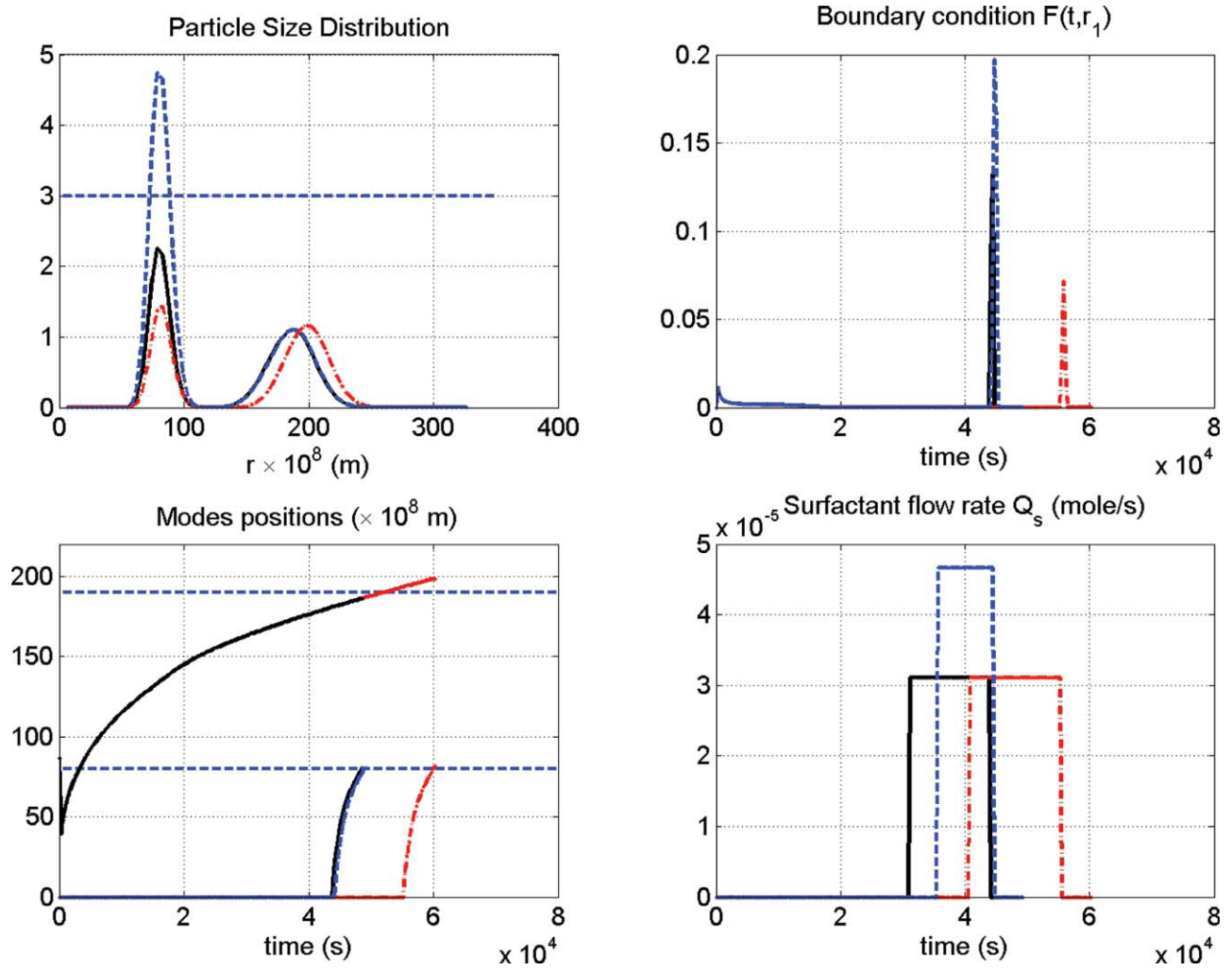

Figure 12. Same illustration as Figure 10 using different desired PSD (first batch in red-dotted, second batch in (red-dotted) and third batch in black-solid line).

Note how the behavioral model enables to capture both the modes positions as well as the amplitude of the latest mode. More precise model of the amplitude may increase the precision of the goal achievement. [Color figure can be viewed in the online issue, which is available at www.interscience.wiley.com.]

additional manipulated variables than the only surfactant flow rate that is used in this work.

Acknowledgments

Part of this work has been supported by the French ANR Grant Capteurs Logiciels Plug & Play.

Notation

a_{sp} = surface area of particles covered by a single surfactant molecule (68×10^{-18} dm^2)
a_{sd} = surface area of droplets covered by a single surfactant molecule (68×10^{-18} dm^2)
CMC = critical Micellar Concentration (5.17×10^{-4} mol/dm^3)
D_p = diffusion coefficient for monomers in particles (1×10^{-15}dm^2/s)
D_w = diffusion coefficient for monomers in water (1.7×10^{-7} dm^2/s)
$[E]$ = concentration of radicals susceptible to enter polymer particles (mol/dm^3)
f = efficiency of radical decomposition (0.6) (−)
f_{em} = efficiency of radical entry into micelles (1×10^{-5}) (−)
f_{ep} = efficiency of radical entry into particles (0.01) (−)
$G(r, t)$ = particle growth rate (dm/s)
$[I]$ = residual initiator concentration (mol/dm^3)
$[IM_i]$ = aqueous phase concentration of oligomeric radicals of degree i (mol/dm^3)
j_{crit} = the chain length at which the radicals become insoluble in water and principate (10) (−)
k_d = initiator decomposition rate coefficient (4.3×10^{-5} s^{-1})
k_{di} = diffusion rate of monomeric radicals of type i to the aqueous phase (s^{-1})
k_{desi} = coefficient of desorption of monomeric radicals of type i (s^{-1})
$k_{ep}(r)$ = coefficient of the radical entry rate into particles (dm^3/mol/s)
k_{em} = coefficient of the rate of radical entry into micelles (dm^3/mol/s)
K_{p11} = coefficient of BuA propagation at 70C (40,400 dm^3/mol/s)
K_{p22} = coefficient of MMA propagation (1050 dm^3/mol/s)
K_{p12} = propagation rate coefficient of BuA with an MMA radical ($K_{p11}/r_1(0.315) = 1.2 \times 10^5$dm^3/mol/s)
K_{p21} = propagation rate coefficient of MMA with a BuA radical ($K_{p22}/r_2(2.64) = 397.7$ dm^3/mol/s)

K_1^P = coefficient of BuA partitioning between polymer particles and the aqueous phase (44) (−)
K_2^P = coefficient of MMA partitioning between polymer particles and the aqueous phase (78) (−)
K_{rad1}^P = partitioning coefficient of BuA radicals between polymer particles and the aqueous phase (781) (−)
K_{rad2}^P = partitioning coefficient of MMA radicals between polymer particles and the aqueous phase (744) (−)
K_1^d = coefficient of BuA partitioning between monomer droplets and the aqueous phase (38) (−)
K_2^d = coefficient of MMA partitioning between monomer droplets and the aqueous phase (64) (−)
k_{t11}^j = coefficient of termination of BuA radicals in phase j (1×10^8 dm^3/mol/s)
k_{t22}^k = coefficient of termination of MMA radicals in phase j (2.9×10^7 dm^3/mol/s)
k_{t12}^j = coefficient of termination of an MMA radical with a BuA radical in phase j ($k_{t21} = \sqrt{k_{t11}\kappa_{t22}}$ dm^3/mol/s)
k_{tr11}^P = coefficient of transfer to BuA in the polymer particles (1.99 dm^3/mol/s)
k_{tr22}^P = coefficient of transfer to MMA in the polymer particles (1.9×10^{-2} dm^3/mol/s)
MW_{m1} = molecular weight of BuA (0.128 kg/mol)
MW_{m2} = molecular weight of MMA (0.100 kg/mol)
$[M_i^j]$ = concentration of monomer i in phase j (mol/dm^3)
[Mic] = concentration of micelles (mol/dm^3)
$n(r, t)$ = number of moles of particles of size between r and $r + dr$ at time t (mol)
$\bar{n}(r, t)$ = average number of radicals in particles of size r at time t
n_{agg} = micellar aggregation number (average number of surfactant molecules in micelles) (60) (−)
N_A = Avogardo's number (mol^{-1})
N_{mi} = number of moles of free monomer in the reactor (mol)
N_S = total number of moles of surfactant in the reactor (mol)
P_i^j = time averaged probability that the ultimate unit of an active chain in phase j be of type i
Q_I = flow rate of initiator (mol/s)
Q_{mi} = flow rate of monomer i (mol/s)
Q_s = flow rate of surfactant (mol/s)
r = particles radius (dm)
r_{mic} = radius of micelles (2.6×10^{-8}dm)
r_{nuc} = nucleation radius (r_{mic}dm)
r_d = radius of the monomer droplets (1×10^{-4}dm)
r_s = swollen particles radius (dm)
$\Re_n$ = nucleation rate (mol/s)
$\Re_{n-hom}$ = homogeneous nucleation rate (mol/s)
$\Re_{n-mic}$ = micellar nucleation rate (mol/s)
$R_{pi}^j(t)$ = polymerization rate of monomer i in phase j (mol/s)
S_{par} = total particle surface (dm^2)
$[T]$ = total concentration of radicals in the aqueous phase (mol/dm^3)
V^w = aqueous phase volume (dm^3)
V^d = droplets volume (dm^3)
V^P = particles volume (dm^3)
V_i^w = volume of monomer i in the aqueous phase (dm^3)
V_i^d = volume of monomer i in the monomer droplets (dm^3)
V_i^p = volume of monomer i in the polymer particles (dm^3)
V_w^w = water volume in the aqueous phase (dm^3)
V_p^P = polymer volume in the polymer particles (dm^3)
z = critical chain length at which polymer radicals can enter polymer particles or micelles causing micellar nucleation (5) (−)
μ = number of moles of radicals in the polymer particles (mol)
ρ_1 = density of BuA (0.857 kg/dm^3)
ρ_2 = density of MMA (0.916 kg/dm^3)
ρ_{p1} = density of poly BuA (1.08 kg/dm^3)
ρ_{p2} = 2 = density of poly MMA (1.15 kg/dm^3)
υ_p = volume of a single polymer particle (dm^3)

Literature Cited

1. Geurts J, Lammers M. The effect of bimodality of the particle size distribution on film formation of latices. *Colloid Surf A*. 1996;303: 108–295.
2. Berend K, Richtering W. Rheology and diffusion of concentrated monodisperse and bidis-perse polymer latices. *Colloid Surf*. 1995; 119:99–101.
3. Schneider M, Claverie J, Graillat C, McKenna T. High solids content emulsions. I. A study of the influence of the particle size distribution and polymer concentration on viscosity. *J Appl Polym Sci*. 2002;84:1878–1896.
4. Semino D, Ray W. Control of systems described by population balance equations-I. Contrability analysis. *Chem Eng Sci*. 1995;50(11): 1805–1824.
5. Semino D, Ray W. Control of systems described by population balance equations-II. emulsion polymerization with constrained control action. *Chem Eng Sci*. 1995;50(11):1825–1839.
6. Elizalde O, Leal G, Leiza J. Particle size distribution measurements of polymeric dispersions: A comparative study. *Part Part Syst Charact*. 2000;17:236–243.
7. Schneider M, McKenna TF. Comparative study of methods for the measurement of particle size and size distribution of polymeric emulsions. *Part Part Syst Charact*. 2000;19:28–37.
8. Santos J, Martins C, Fortuny M, Santos A, Turmine M, Graillat C, McKenna T. In-line and in situ monitoring of ionic surfactant dynamics in latex reactors using conductivity measurements and ion-selective electrodes. *Ind Eng Chem Res*. 2007;46:1465–1474.
9. Abedini H, Shahrokhi M. Inferential closed-loop control of particle size distribution for styrene emulsion polymerization. *Chem Eng Sci*. 2008;63:2378–2390.
10. Kiparissides C. Challenges in particulate polymerization reactor modeling and optimization: A population balance perspective. *J Process Control*. 2006;16:205–224.
11. Crowley T, Meadows E, Kostoulas E, Doyle F. Control of particle size distribution described by a population balance of semibatch emulsion polymerization. *J Process Control*. 2000;10:419–432.
12. Immanuel C, Doyle FJ III. Open-loop control of particle size distribution in semi-batch emulsion copolymerization using a genetic algorithm. *Chem Eng Sci*. 2002;57:4415–4427.
13. Immanuel C, Doyle FJ III. Hierarchical multiobjective strategy for particle-size distribution control. *AIChE J*. 2003;49(9):2383–2399.
14. Alhamad B, Romagnoli J, Gomes V. On-line multi-variable predictive control of molar mass and particle size distributions in free-radical emulsion copolymerization. *Chem Eng Sci*. 2005;60:6596–6606.
15. Zeaiter J, Romagnoli J, Gomes V. On-line control of molar mass and particle-size distributions in emulsion polymerization. *AIChE J*. 2006;52:1770–1779.
16. Dokucu M, Park M, Doyle FJ III. Multi-rate model predictive control of particle size distribution in a semibatch emulsion copolymerization reactor. *J Process Contr*. 2008;18:105–120.
17. Flores-Cerillo J, MacGregor JF. Control of particle size distributions in emulsion semibatch polymerization using mid-course correction policies. *Ind Eng Chem Res*. 2002;41:1805–1814.
18. Doyle FJ III, Harrison C, Crowley T. Hybrid model-based approach to batch-to-batch control of particle size distribution in emulsion polymerization. *Comp Chem Eng*. 2003;27:1153–1163.
19. Dokucu M, Doyle FJ III. Batch-to-batch control of characteristic points on the PSD in experi- mental emulsion polymerization. *AIChE J*. 2008;54:3171–3187.
20. Immanuel C, Wand Y, Bianco N. Feedback controllability assessment and control of particle size distribution in emulsion polymerization. *Chem Eng Sci*. 2008;63:1205–1216.
21. Willems JC. Paradigms and Puzzles in the Theory of Dynamical Systems. *IEEE Trans Automat Contr*. 1991;36.
22. Fortuny M, Graillat C, McKenna T. Modeling the nucleation stage during batch emulsion polymerization. *AIChE J*. 2005;51.
23. O'Toole JT. Kinetics of emulsion polymerization. *J Appl Polym Sci*. 1965;9:1291–1297.
24. Li CG, Brooks BW. Prediction of the average number of radicals per particle for emulsion polymerization. *J Polym Sci Part A: Polym Chem*. 1993;31:2397–2402.

Appendix: Process Model

Population balance equations

The pseudo-bulk model is used to represent the particle size distribution (PSD) in this system since it is valid for large

particles in which more than one free radical can co-exist for a significant period. This model is described by two partial differential equations: one equation represents the evolution of the PSD with time and the second equation represents the number of radicals in the considered particles as follows:

$$\frac{\partial n(r,t)}{\partial t}+\frac{\partial (n(r,t)G(r))}{\partial r}=\Re_n\delta(r-r_{\text{nuc}})+\Re_{\text{coagulation}} \quad \text{(A1)}$$

$$\frac{\partial \bar{n}(r,t)}{\partial t}=\acute{\Re}_{\text{entry}}-\acute{\Re}_{\text{desorption}}-2\acute{\Re}_{\text{termination}} \quad \text{(A2)}$$

The particle density $n(r, t)dr$ is defined as the number of moles of particles of size between r and $r + \delta r$ at time t, $\Re_n$ is the rate of nucleation and $\delta(r - r_{\text{nuc}})$ is the dirac delta function which is unity at $r = r_{\text{nuc}}$ and zero elsewhere which represents the boundary conditions, $G(r, t)$ is the particle growth $\left(G(r,t)=\frac{dr}{dt}\right)$, $\acute{\Re}_{\text{entry}}, \acute{\Re}_{\text{desorption}}$ and $\acute{\Re}_{\text{termination}}$ are the total ra radical entry, desorption and termination within a single particle of size between r and $r + \delta r$ respectively. Based on the solution of the modified Bessel function of the first kind of Eq. (31) proposed in Ref. 23 the following semi-theoretical expression has been proposed in Ref. 24 to determine $\bar{n}(r,t)$:

$$\bar{n}(r,t)=\frac{2H}{m+\left(m^2+\frac{8H(2H+m)}{2H+m+1}\right)^{1/2}} \quad \text{(A3)}$$

where

$$m=\bar{k}_{\text{des}}N_A\frac{v_p}{k_t^p} \quad ; \quad H=k_{\text{ep}}(r)N_Av_p\frac{[E]}{k_t^p} \quad v_p=\frac{4}{3}\pi r_s^3 \quad \text{(A4)}$$

Micellar ($\Re_{n-\text{mic}}$) and homogeneous ($\Re_{n-\text{hom}}$) nucleations cause formation of very small parti- cles. The total nucleation rate ($\Re_n=\Re_{n-\text{hom}+\Re_{n-\text{mic}}}$) acts therefore as a boundary condition of Eq. (31). This results in a Dirichlet condition as follows:

$$n(r_{\text{nuc}},t)=\frac{\Re_n(t)}{G(r_{\text{nuc}})} \quad \text{(A5)}$$

with,

$$\Re_{n-\text{mic}}(t)=k_{\text{em}}[Mic][E]V^w \quad \text{(A6)}$$

$$\Re_{n-\text{hom}}(t)=\varepsilon_1[IM_{j_{\text{crit}}}]V^w \quad \text{(A7)}$$

where $[E]=\sum_{i=z}^{j_{\text{crit}}-1}$ is the concentration of radicals susceptible to enter polymer particles and ($k_{\text{em}} = 4\pi r_{\text{mic}}N_AD_wf_{\text{em}}$) is the rate coefficient of particle nucleation depending on the radius of micelles (r_{mic}). In this model, particles were assumed to be colloidally stable, therefore coagulation was not considered.

Aqueous phase reactions

Ammonium persulfate was used as initiator in this work. The polymerization process starts by the initiator decomposition (I) in the aqueous phase producing primary radicals (IM_1) that react with monomer molecules (M) to generate oligomeric radicals (IM_i):

$$\frac{d([I]V^w)}{dt}=Q_I-k_d[I]V^w \quad \text{(A8)}$$

where V^w is the volume of the aqueous phase, Q_I is the initiator flow rate and $[I]$ is the initiator concentration. The stationary state hypothesis of radicals leads to:

$$[IM_1]=\frac{1}{\varepsilon_2}\left(2fk_d[I]+\frac{1}{V^w}\int_{r_{nuc}}^{\infty}\bar{k}_{\text{des}}(r)n(r,t)\bar{n}(r,t)dr\right) \quad \text{(A9)}$$

$$[IM_i]_{i=2-(z-1)}=\frac{\varepsilon_1}{\varepsilon_2}[IM_{i-1}] \quad \text{(A10)}$$

$$[IM_i]_{i=z-j_{\text{crit}}}=\frac{\varepsilon_1}{\varepsilon_2+\varepsilon_3}[IM_{i-1}] \quad \text{(A11)}$$

where z is the critical chain length at which polymer radicals can enter polymer particles or micelles (micellar nucleation), j_{crit} is the chain length at which the radicals become insoluble in water and precipitate therefore as new particles (homogeneous nucleation) and

$$\begin{aligned}
\varepsilon_1&=(k_{p11}^{\text{w}}P_1^{\text{w}}+k_{p21}^{\text{w}}P_2^{\text{w}})[M_1^{\text{w}}]+(k_{p12}^{\text{w}}P_1^{\text{w}}+k_{p22}^{\text{w}}P_2^{\text{w}})[M_2^{\text{w}}]\\
\varepsilon_2&=\varepsilon_1+k_t^{\text{w}}[T]\\
\varepsilon_3&=\frac{1}{V^{\text{w}}}\int_{r_{\text{nuc}}}^{\infty}k_{ep}(r)n(r,t)dr+k_{\text{em}}[Mic]\\
k_t^j(t)_{j=w,P}&=k_{t11}^jP_1^{j2}+2k_{t12}^jP_1^jP_2^j+k_{t22}^jP_2^{j2}
\end{aligned} \quad \text{(A12)}$$

where $[T]$ is the total concentration of radicals in the aqueous phase defined by:

$$[T]=\sum_{i=1}^{j_{\text{crit}}-1}[IM_i]$$

The desorption rates of monomeric radicals are given by:

$$\begin{aligned}
\bar{k}_{\text{des}}(t)&=k_{\text{des1}}+k_{\text{des2}}\\
k_{\text{des}i}(t)_{i=1,2}&=\frac{(k_{tr1i}^PP_1^P+k_{tr2i}^PP_2^P)[M_i^P]k_{di}}{k_{di}\beta_i+K_{pi1}[M_1^P]+K_{pi2}[M_2^P]}\\
k_{\text{di};i=1,2}&=\frac{3D_w}{K_{radi}^Pr_s^2\left(1+\frac{2D_w}{K_{radi}^PD_p}\right)}\\
\beta_i(t)_{i=1,2}&=\\
&\frac{K_{pi1}^w[M_1^w]+K_{pi2}^w[M_2^w]+(k_{ti1}^wP_1^w+k_{ti2}^wP_2^w)[T]}{\frac{1}{V^w}\int_{r_{\text{nuc}}}^{\infty}k_{\text{ep}}(r)n(r,t)dr+k_{pi1}^w[M_1^w]+k_{pi2}^w[M_2^w]+[T](k_{ti1}^wP_1^w+k_{ti2}^wP_2^w)}
\end{aligned}$$

$$k_{\text{ep}}(r)=4\pi r_sN_AD_wf_{\text{ep}} \quad \text{(A13)}$$

Monomer material balance and partitioning between the phases

The copolymerization of methyl methacrylate (MMA) and butyl acrylate (BuA) was considered in this work. The material balance of monomers taking into account the reaction rate in both phases is given by:

$$\begin{aligned}
\frac{dN_{\text{mi}}(t)}{dt}_{i=1,2}&=Q_{mi}(t)-R_{\text{pi}}^P(t)-R_{\text{pi}}^w(t)\\
\frac{dN_{\text{mi}}^T(t)}{dt}_{i=1,2}&=Q_{mi}(t)
\end{aligned} \quad \text{(A14)}$$

where $N_{mi}(t)$ is the residual number of moles of monomer i, Q_{mi} is the monomer flow rate i, $N_{\text{mi}}^T(t)$ is the total number

of moles of monomer i introduced to the reactor at time t and:

$$\begin{aligned}
&R_{pi}^{P}(t)_{i=1,2} = \mu[M_i^P]F_i^P \\
&\mu = \int_{r_{\text{unc}}}^{\infty} \bar{n}(r,t)n(r,t)dr \\
&R_{\text{pi}}^{w}(t)_{i=1,2} = [T][M_i^w]F_i^w \\
&F_i^j(t)_{i=1,2;j=P,w} = K_{p1i}P_1^j + K_{p2i}P_2^j \\
&P_1^j(t)_{j=P,w} = \frac{K_{p21}[M_i^j]}{K_{p21}[M_1^j] + K_{p12}[M_2^j]} \\
&P_2^j(t)_{j=P,w} = 1 - P_1^j(t) \\
&[M_i^j](t)_{i=1,2;j=w,P} = \frac{\rho_i V_i^j}{MW_i V_j}
\end{aligned} \tag{A15}$$

Particle growth can now be calculated as:

$$G(r,t) = \frac{\frac{MW_1}{\rho_{p1}}[M_1^P]F_1^P + \frac{MW_2}{\rho_{p2}}[M_2^P]F_2^P}{4\pi r_s^2 N_A} \tag{A16}$$

Monomer partitioning between the different phases is obtained by solving numerically the following 9 algebraic equations:

$$\begin{aligned}
&V_i^P(t)_{i=1,2} = \frac{V_i}{\frac{K_i^d}{K_i^P}\frac{V^d}{V^P} + \frac{1}{K_i^P}\frac{V^w}{V^P} + 1} \\
&V_i^d(t)_{i=1,2} = \frac{K_i^d}{K_i^P}\frac{V^d V_i^P}{V^P} \\
&V_i^w(t)_{i=1,2} = \frac{V^w}{K_i^P}\frac{V_i^P}{V^P} \\
&V^P(t) = V_1^P + V_2^P + V_p^P \\
&V^d(t) = V_1^d + V_2^d \\
&V^w(t) = V_1^w + V_2^w + V_w^w
\end{aligned} \tag{A17}$$

where $V_p^P = (N_{m1}^T(t) - N_{m1}(t))\frac{MW_1}{\rho_{p1}} + (N_{m2}^T(t) - N_{m2}(t))\frac{MW_2}{\rho_{p2}}$.

Surfactant material balances and micelle concentration

The surfactant DISPONIL FES 32 was considered in this work. The surfactant is assumed to be introduced at a flow rate Q_S(mol/s) and therefore the total number of moles of surfactant in the reactor is:

$$\frac{dN_S(t)}{dt} = Q_s(t) \tag{A18}$$

The concentration of micelles is calculated using the following expression:

$$[Mic](t) = \max\left(0, \frac{\frac{N_S}{V_w^w} - CMC - \frac{S_{\text{part}}}{V_w^w a_{\text{sp}} N_A} - \frac{3V^d}{V_w^w a_{\text{sd}} r_d N_A}}{n_{\text{agg}}}\right) \tag{A19}$$

where CMC is the critical micelle concentration, n_{agg} is the aggregation number for the surfactant and S_{par} is the total particles surface:

$$S_{\text{par}}(t) = 4\pi N_A \int_{r_{\text{nuc},t}}^{\infty} n(r,t) r_S^2 dr \tag{A20}$$

where r_s is the swollen particle radius given by

$$r_s(t) = r\left(\frac{1}{1 - [M_1^P]\frac{MW_1}{\rho_1} - [M_2^P]\frac{MW_2}{\rho_2}}\right)^{1/3} \tag{A21}$$

Manuscript received Sept. 24, 2009, and revision received Oct. 27, 2009.